How to cite: *Angew. Chem. Int. Ed.* **2023,** *62,* e202217917
International Edition: doi.org/10.1002/anie.202217917
German Edition: doi.org/10.1002/ange.202217917

Metallacycles

A Fourfold Gold(I)–Aryl Macrocycle with Hyperbolic Geometry and its Reductive Elimination to a Carbon Nanoring Host

*Niklas Grabicki, Sergey Fisher, and Oliver Dumele**

Abstract: An ethylene glycol-decorated [6]cyclo-*meta*-phenylene (CMP) macrocycle was synthesized and utilized as a subunit to construct a fourfold Au^{I}_{2}–aryl metallacycle with an overall square arrangement. The corners consist of rigid dinuclear gold(I) complexes previously known to form only triangular metallacycles. The interplay between the conformational flexibility of the [6]CMP macrocycle and the rigid dinuclear gold(I) moieties enable the square geometry, as revealed by single-crystal X-ray diffraction. The formation of the gold complex shows size-selectivity compared to an alternative route using platinum(II) corner motifs. Upon reductive elimination, an all-organic ether-decorated carbon nanoring was obtained. Investigation as a host for the complexation of large guest molecules with a suitable convex π-surfaces was accomplished using isothermal NMR binding titrations. Association constants for [6]cycloparaphenylene ([6]CPP), [7]CPP, C_{60}, and C_{70} were determined.

Carbon nanotubes (CNTs) are based on a hexagonal honeycomb lattice of sp^2-carbon atoms. They can be semiconducting or metallic, depending on the orientation of the lattice with respect to the nanotube axis.[1,2] Due to the large interest in this exciting class of materials, several methods have been developed to access their shortest possible repeating units, such as cyclo-*para*-phenylenes (CPPs) or zigzag carbon nanobelts.[3–9] While this can be seen as an endeavor towards the diameter-selective bottom-up synthesis of CNTs, these aromatic macrocycles possess unique properties on their own. Their radially oriented π-orbitals and inherent strain energy lead to distinct photophysical properties compared to their corresponding linear structures.[10–12] These properties can be altered by the implementation of hetero- or polycyclic aromatic moieties.[13–18] Additionally, the shape persistence and the convex–concave π-surface of CPPs and other related macrocycles has led to multiple supramolecular host–guest studies, most prominently with fullerenes.[19–24] Other applications in a variety of research areas, such as sensing or imaging, have also been investigated.[25–27] Existing synthetic methodologies of ring or belt formation have been applied to extend the possible molecular shapes in the areas of macrocycles,[28] belts,[7–9,29–31] lemniscates,[26,32,33] and cages.[34–36] Larger cyclic nanorings, such as molecular phenine nanotubes,[37–39] cyclo[*n*]porphyrins,[40] or cyclo[*n*]hexabenzocoronenes[41] were constructed from extended molecular subunits as building blocks in a macrocyclization strategy. For example, [6]cyclo-*meta*-phenylene ([6]CMP, a phenine subunit) was employed as monomer for the synthesis of expanded CPP-type carbon nanorings by a Pt-mediated cyclization.[38,39,42] These phenine nanorings, pioneered by Isobe and co-workers, are curved yet almost strain-free due to the conformational flexibility of the subunits and their overall large diameter. However, utilizing reversible Pt-complexation often resulted in complex product mixtures typically containing various ring sizes of the reductively eliminated carbon nanorings.[41–46] We were intrigued by a synthetic protocol for carbon nanorings based on an Au^{I}-macrocyclization with a promising size-selectivity by Tsuchido, Osakada, and co-workers.[47] This approach is limited to triangular geometries using rigid rod-shaped aromatic subunits.[48] In contrast, we aimed to explore flexible polycyclic subunits to access carbon nanorings bearing a large cavity for host–guest chemistry.

Here we present a size-selective strategy to obtain highly functionalized carbon nanorings with a large inner cavity defined by sterically demanding ethylene glycol groups at the edges for the supramolecular binding of guest molecules.[49] Previously, we reported a strategy confining the inner space of strained cyclo[*n*]pyrenylene nanorings by ethylene glycol functionalization of diketone moieties.[46] Following this approach, we now used an extended ethylene glycol-functionalized subunit **A** in an Au^{I}-macrocyclization protocol by Tsuchido, Osakada, and co-workers (Scheme 1).[47] In this approach, a dinuclear gold(I) complex is used as a corner motif to subsequently obtain an extended carbon nanoring as supramolecular host.[50]

The rich chemistry developed on [*n*]CMPs (with $n = 6$, 8, 10), first synthesized by Staab[51] and later used by Cram as spherands,[52] make these planar aromatic macrocycles an ideal starting point in the construction of larger structures.[53–55] Diboronic ester **5** was synthesized on a multi-gram scale within three steps starting from commercially available 9,10-phenanthrenequinone (Figure 1 and Section S2).[56] One-pot macrocyclization of diboronic ester **5** and 1,3-dibromobenzene led to the formation of bisacetal

[*] N. Grabicki, S. Fisher, O. Dumele
Department of Chemistry, Humboldt-Universität zu Berlin
Brook-Taylor-Straße 2, 12489 Berlin (Germany)
E-mail: oliver.dumele@hu-berlin.de
Homepage: www.dumelelab.com

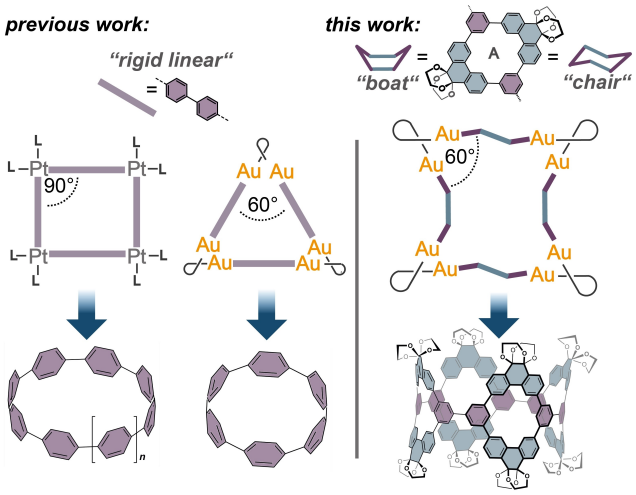

Scheme 1. Comparison of the macrocyclic geometries accessible with Pt^{II} (L = ligand) or Au^{I} complexes, which function as templating agents. Conformational flexibility of the [6]CMP unit forms a fourfold macrocycle.

interphenylene-bridged [6]CMP derivative **4** (Figure 1; roman numeral I; see also Figure S1 Section S2). Due to the reduced symmetry of **4**, the one-pot macrocyclization of the unequal building blocks **5** and 1,3-dibromobenzene is impeded compared to parental [6]CMP.[57] We also explored an alternative step-wise synthetic route and different substitution patterns of **4**, which resulted in similar overall yields toward **3** (Section S2). Examination of the single-crystal structure of **4** showed that the macrocycle establishes an overall chair conformation analogous to cyclohexane.[79] A dihedral scan at the DFT:B3LYP/6-31G(d,p) level of theory revealed an energy difference of 0.3 kcal mol^{-1} between a boat and a chair conformation of **4** (Figure 2).

A small energy difference between those two conformers is crucial as the [6]CMP moiety must adopt a boat conformation in the desired final nanoring **1** (Figure S21). The energetic barrier $\Delta G^{\ddagger}$ for the chair-to-boat isomerization is 3.1 kcal mol^{-1} allowing fast exchange between the energetically similar conformers (Figure 2). For comparison, the chair→twist-boat isomerization of deuterated cyclohexane (C_6HD_{11}) at 25 °C is too fast to be detected on the NMR time scale and has a barrier of ca. 10 kcal mol^{-1}.[58] Subsequent regioselective Ir-catalyzed C–H borylation of **4** gave diboronic ester **3**. Initial exploration of established platination methods[5,59,60] to form a Pt-macrocycle **2-Pt$_n$** and reductive elimination gave a mixture of various ring sizes. We isolated the fourfold nanoring **1** and the fivefold nanoring **1-v** by tedious recycling gel permeation chromatography (*r*GPC) in < 1 % yield, each (Figures S52–S55). Formation of several ring sizes and low yields are common features observed in other examples following the platinum-mediated macrocyclization, including our own ethylene glycol-functionalized cyclo[*n*]pyrenylenes.[41,42,44,61,62] We therefore turned to gold(I)-mediated macrocyclization methods and targeted a cyclotrimerization strategy with the initial aim to form a triangular-shaped macrocycle.[47,48]

Reaction of [6]CMP diboronic ester **3** with [Au_2Cl_2-(dcpm)] (dcpm = bis(dicyclohexylphosphino)methane) produced an unexpected fourfold gold macrocycle **2-Au** in 33 % yield after *r*GPC. No additional defined fractions of larger ring sizes were detected during preparative *r*GPC resulting in a straight forward separation. Comprehensive characterization of **2-Au** by NMR spectroscopy was not possible due to broad signals and limited solubility. Aiming for increased dynamics of the system we performed variable temperature (VT) NMR experiments, yet did only observe degradation

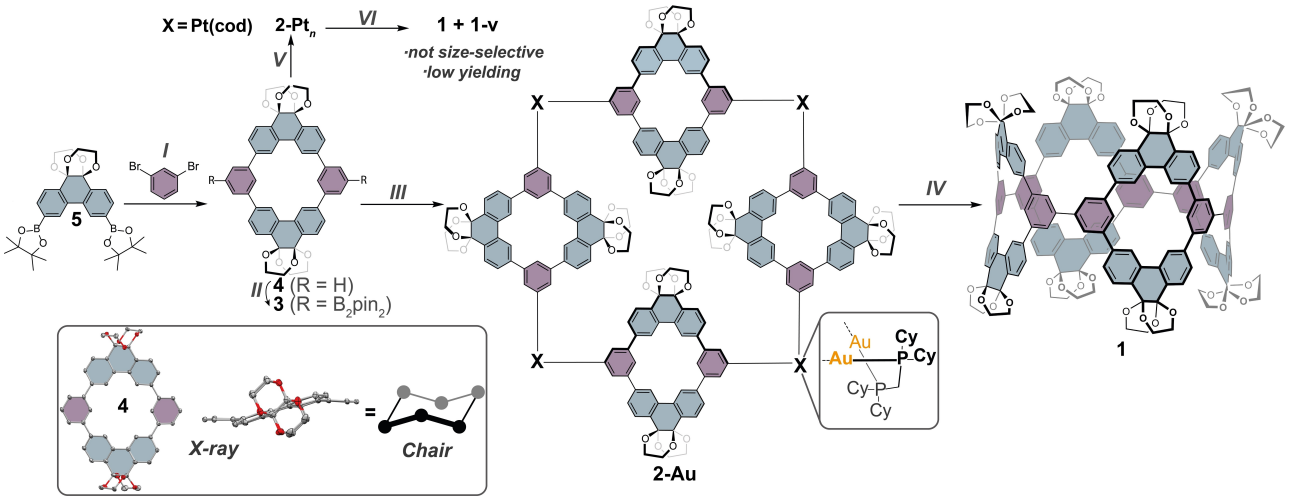

Figure 1. Synthesis of **1**: I) $Pd(OAc)_2$, SPhos, K_3PO_4, 60 °C, 4 h, 7 %; II) 4,4′-di-*tert*-butyl-2,2′-bipyridine, $[Ir(OMe)(COD)]_2$, bis(pinacolato)diboron, 1,4-dioxane, 120 °C, 18 h, 73 %; III) [Au_2Cl_2(dcpm)], Cs_2CO_3, toluene/EtOH/H_2O (4 : 1 : 1), 50 °C, 20 h, 33 %; IV) $PhICl_2$, DMF, −50 °C to 25 °C, 20 h, 20 %; V) [$PtCl_2$(COD)], CsF, THF, 66 °C, 24 h, not isolated; VI) $P(Ph_3)$, toluene, 100 °C, 22 h, < 1 %, over two steps for **1** and **1-v**; dcpm = bis(dicyclohexylphosphino)methane. The inset shows the SXRD structure of **4** top view and side view, as well as a schematic representation of a six-membered ring in the chair conformation.

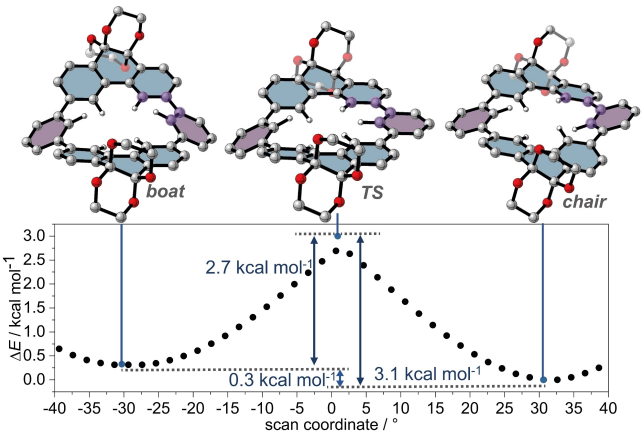

Figure 2. The optimized structures of **4** in the boat, transition state (TS), and chair conformation at the DFT:B3LYP/6-31G(d,p) level of theory. Initial dihedral scan coordinate (black dots) with energetic positions of unrestricted optimized structures of boat, TS, and chair (blue dots). The scan was performed on the dihedral bond (highlighted in purple). All hydrogen atoms, except the inner ones of [6]CMP, are omitted for clarity.

of **2-Au** at 65 °C to subunit **4** (Figures S109–S110). We cannot assure complete bulk purity but repeatedly observed the formation of single-crystalline material exhibiting uniform unit cell parameters (Figure 3a, Figures S6–S9)). Macrocycle **2-Au** displays an unusual geometry with two [6]CMP moieties in a chair conformation and two [6]CMP moieties in a boat conformation, which produces hyperbolic edges of the complex. This equal mixing of both conformers in the same structure leads to an unusual geometry of the overall macrocycle. The sum of the angles deviates from the typical (Euclidian) 360°, characteristic for hyperbolic geometries. The four Au_2(dcpm) corners show torsion angles along the C–Au···Au–C bonds of 53° and 48° (Figure S8), while aurophilic interactions between the Au^I···Au^I centers, bridged by a dcpm ligand, are present with distances of 3.124 Å and 3.150 Å (Figure S8). These values are in the same range as for earlier reported triangular structures and determine the hyperbolic geometry of this fourfold macrocycle with corner angles significantly below 90°.[47,48] This demonstrates the rigidity between the two Au^I centers imposed by the aurophilic interactions in this complex while flexibility originates from the [6]CMP subunits (torsional freedom around the phenyl–phenanthrenyl bonds, Figure 3a). Complex **2-Au** has two chirality axes formed by the twisted Au_2P_2C five-membered rings of the two corners in the asymmetric unit. X-ray crystallography revealed one *M* and one *P* chirality axis (Figure 3a). The polarized C–H bonds of the ethylene glycol groups in the center of **2-Au** engage in several C–H···O hydrogen bonds with heavy atom distances between 3.126 Å and 3.409 Å (Figure S10). We assume that this cooperative interaction network stabilizes the overall structure of **2-Au** while preventing inner void space. The oxidative chlorination of complex **2-Au** induced the reductive elimination to final carbon nanoring **1** in 20 % yield with definite size selectivity (as observed by *r*GPC of the crude reaction mixture, see Figure S67). Prior silica gel column chromatography of the reaction mixture allows to recover the gold precursor [Au_2Cl_2(dcpm)]. Unambiguous structural proof was obtained by single-crystal X-ray analysis of **1** revealing its porous molecular structure with several resolved $CHCl_3$ and benzene solvent molecules (Figures S11 and S16) due to Cl_3C–H···O_{host} hydrogen bonds (3.2–3.5 Å heavy atom distance) and C–Cl···O_{host} halogen bonds (3.0 Å).[63,64] The central diameter of ca. 16 Å is comparable to that of [12]CPP and the packing shows a slipped-stacked tubular arrangement, presumably due to the sterically demanding ethylene glycol groups that prevent a self-filling herringbone assembly (Figure S13–S15).

The UV/Vis absorption maximum λ_{max} of **1** at 261 nm shows only a small red shift compared to its monomer **4** at 259 nm due to the poorly conjugated *meta*-connectivity between the individual CMP-panels. Similar to [*n*]CPP-type macrocycles, a small red-shifted shoulder can be observed for **1**. Considering the oscillator strengths (f_{os}) of the calculated transitions, this shoulder at 292 nm is assigned to a Laporte-forbidden HOMO–LUMO transition (Table S1).[10,65,66] It is a common feature observed for CPPs and originates from the high molecular symmetry retained in their molecular orbital structure.[12] The main absorption band at 261 nm of **1** does not correspond to the HOMO→

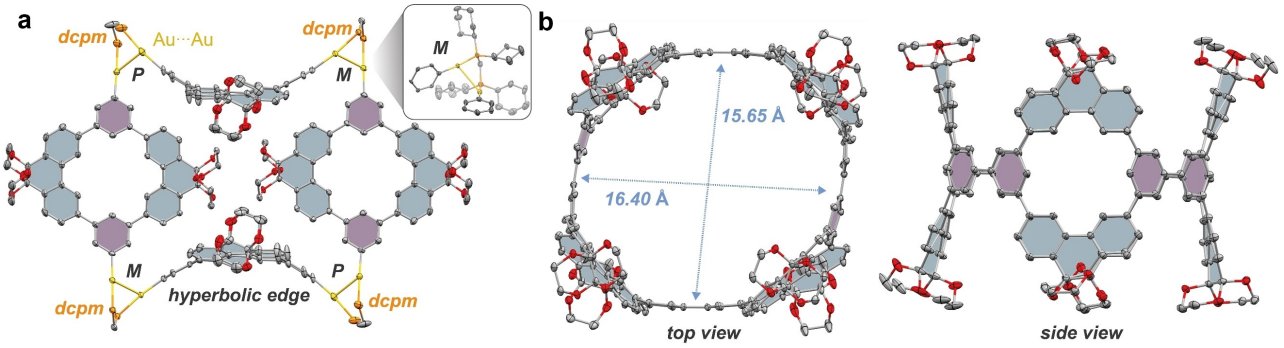

Figure 3. a) Single-crystal X-ray structure of gold macrocycle **2-Au** with an inset showing the dcpm ligand and the chirality of the gold corner and b) all-organic macrocycle **1**. H-atoms, dcpm ligands and solvent molecules are omitted for clarity, thermal ellipsoids are shown at 50 % probability at 100 K. dcpm = bis(dicyclohexylphosphino)methane.[79]

LUMO+1 or HOMO→LUMO+2 transition as it is typically observed for [*n*]CPPs, but is composed of multiple transitions between various energy levels (Figure S24, Table S10). Macrocycle **1** and monomer **4** show large apparent Stokes shifts of 87 and 67 nm (0.76 and 1.21 eV), respectively (with regard to the forbidden HOMO–LUMO transition for **1**), which is an important feature for future sensing applications with nanoring **1**.

The photophysical properties of these CPP-type macrocycles are assigned to their symmetrically curved structure induced by the strain necessary to create the circular arrangement. The strain energy of **1**, calculated using StrainViz,[67] revealed an evenly distributed dihedral strain energy on all twelve biphenyl units within the CMP-panels, but a localized strain energy on the bonds connecting the [6]CMP moieties (red bonds Figure 4b). Nevertheless, the overall strain for **1** is significantly smaller with 9.3 kcal mol^{-1} compared to 48.3 kcal mol^{-1} for [12]CPP.[67] The key for the unusual geometry of organo-metallic macrocycle **2-Au** and the low molecular strain energy of **1** lies in the conformational freedom of subunit **4**.

Macrocycle **1** has an unusually large void volume for a single small molecule with an estimated size of 5500 Å^3 (Figure 5c, blue volume, calculated and visualized using the MS Roll suite implemented in X-Seed[68]). The gate diameter formed by the ethylene glycol groups is smaller compared to the cavity diameter in the center of macrocycle **1**, which motivated us to explore the guest uptake into this confined space (Figures S17–S18, Table S7).[46,49,69,70]

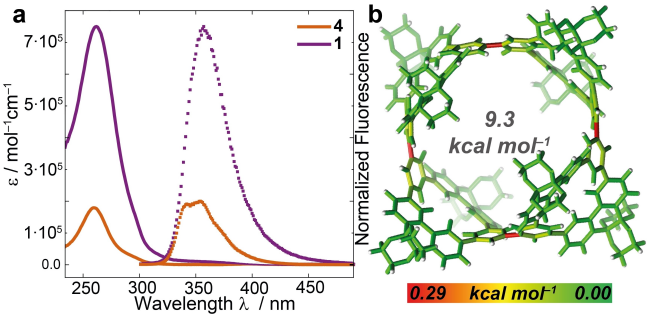

Figure 4. a) UV/Vis absorption (solid lines) and emission (dashed lines) spectra of **4** and **1** (CH_2Cl_2, 25 °C, excitation wavelength 250 nm). b) Molecular strain energy for **1** calculated and visualized using StrainViz (DFT:B3LYP/6-31G(d)).

Previous studies have shown that shape-persistent [*n*]CPPs bind [*n*–5]CPPs and fullerenes selectively.[14,23,37,42,71] The similarity of **1** to [12]CPP, with regard to the cavity diameter, directed us to investigate the binding of [7]CPP through ^{1}H NMR isothermal binding titrations. Upon addition of [7]CPP to **1** in $CDCl_3$ at 25 °C, three sets of protons (H_a, H_d, H_e, Figure 5a) showed a significant change of the chemical shift ($\Delta\delta$) at fast exchange (Figure 5b). Nonlinear least-square curve fitting of the titration data on H_d afforded an association constant (K_a) of 360 M^{-1} (Figure S32). A 1:1 host–guest stoichiometry was confirmed by the stochastic distribution of the corresponding residuals (Figure S33).[72,73]

The downfield shift of proton H_d can be rationalized with the increased magnetic shielding experienced by these protons due to the exposition towards the π-surface of [7]CPP aligning parallel to the walls of **1** in its center. The association constant of **1**···[7]CPP is in the same range as that of [12]CPP···[7]CPP determined by Yamago and co-workers (K_a = 93 M^{-1} in TCE-d_2 at 50 °C).[74] Additionally, we performed isothermal binding titration of **1** and [6]CPP. While earlier investigations found no binding of [*n*]CPPs with [*n*–6]CPPs, we could fit the obtained ^{1}H NMR binding data of proton H_d to obtain K_a = 110 M^{-1}. It is weaker than the association of **1**···[7]CPP due to the size mismatch of **1** and [6]CPP.

We next turned our attention to the inclusion of fullerenes (C_{60}, C_{70}) as guest molecules, because of their shape-complementary convex π-surface. Although macrocycle **1** has a central diameter of 16 Å—slightly too large to efficiently host C_{60} with its mean diameter of 7.1 Å—we determined an association constant of 7.2·10^3 M^{-1} for **1**···C_{60} at 25 °C in *o*-dichlorobenzene-d_4 (DCB-d_4). Compared to the spherical shape of C_{60}, the shape of C_{70} is reminiscent of a rugby football with a short axis of 7.12 Å and a long axis

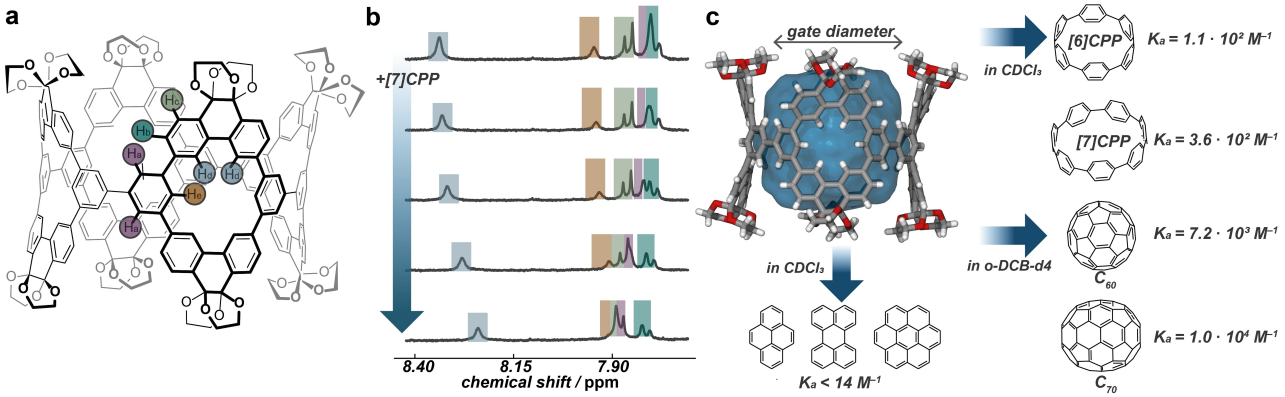

Figure 5. a) Molecular structure of **1**; b) ^{1}H NMR spectrum of **1** upon addition of [7]CPP in the range of 8.40–7.80 ppm in $CDCl_3$ at 25 °C; c) single-crystal X-ray structure of **1** with the visualized void volume (calculated using the MS Roll suite implemented in X-Seed[68]) and the investigated guests with their corresponding association constants (K_a) determined by ^{1}H NMR isothermal binding titration.

of 7.96 Å.[75] As expected, the larger C_{70} can fill more of the void volume of host **1** leading to an increased π-π interaction surface that is reflected in a K_a of 1.0×10^4 M^{-1} (Figure 5c). In comparison, a structurally similar [4]CPP geodesic phenine framework ([4]CPP-GPF) shows binding to C_{70} in the less competitive solvent toluene-d_8 of $K_a = 4.7\times10^4$ M^{-1}.[42] Possible structures of the investigated complexes were disclosed by density functional theory (B3LYP/3-21G level of theory, Figures S25–S28). These structures show that macrocycle **1** binds a variety of guests with large curved π-surfaces, albeit they are not perfectly complementary in size and shape. In contrast, our studies investigating the binding of rigid planar π-aromatic molecules such as pyrene, perylene, or coronene did not show pronounced binding (Figure 5c and S53–S62). We envision **1** as a promising host molecule for future assembly studies with more elaborated guests bearing the potential to achieve large multi-component supramolecular structures.

In summary, we synthesized a metal-organic macrocycle consisting of hyperbolic geometric features that evolved from the unique conformational flexibility of the macrocyclic subunits leading to an unprecedented fourfold Au^I–aryl macrocycle. The reductive elimination to carbon nanoring **1** proceeds with size-selectivity and a remarkable yield of 20 %. The final macrocycle shows binding towards multiple guests with convex π-surfaces. Binding to such large and confined cavities will be of high interest for the sensing of guests with biological relevance, as well as for constructing interlocked molecular topologies. We are confident that our findings bear importance for the design of metal- and all-organic macrocycles and cages.[76–78]

Acknowledgements

We thank Manfred Weiss and his group for assistance at the beamline sector MX14.2 at BESSY-II, Beatrice Cula for crystallographic advice, Dietrich Volmer for access to HR-ESI-MS, Steffen Weidner (BAM) for measurement of HR-MALDI-MS, and Lukas Husarich for the synthesis of the Au_2Cl_2(dcpm) precursor. N.G. was supported by a doctoral fellowship of the Fonds der Chemischen Industrie (FCI) and O.D. thanks the FCI for a generous Liebig scholarship. We are grateful to Stefan Hecht for his continuous support. Open Access funding enabled and organized by Projekt DEAL.

Conflict of Interest

The authors declare no conflict of interest.

Data Availability Statement

The data that support the findings of this study are available in the supplementary material of this article.

Keywords: Cycloparaphenylenes · Host–Guest Systems · Macrocycles · Molecular Recognition · Supramolecular Chemistry

[1] S. Iijima, *Nature* **1991**, *354*, 56–58.
[2] M. S. Dresselhaus, G. Dresselhaus, R. Saito, *Carbon* **1995**, *33*, 883–891.
[3] R. Jasti, J. Bhattacharjee, J. B. Neaton, C. R. Bertozzi, *J. Am. Chem. Soc.* **2008**, *130*, 17646–17647.
[4] H. Takaba, H. Omachi, Y. Yamamoto, J. Bouffard, K. Itami, *Angew. Chem. Int. Ed.* **2009**, *48*, 6112–6116; *Angew. Chem.* **2009**, *121*, 6228–6232.
[5] S. Yamago, Y. Watanabe, T. Iwamoto, *Angew. Chem. Int. Ed.* **2010**, *49*, 757–759; *Angew. Chem.* **2010**, *122*, 769–771.
[6] E. Kayahara, V. K. Patel, S. Yamago, *J. Am. Chem. Soc.* **2014**, *136*, 2284–2287.
[7] K. Y. Cheung, K. Watanabe, Y. Segawa, K. Itami, *Nat. Chem.* **2021**, *13*, 255–259.
[8] Y. Han, S. Dong, J. Shao, W. Fan, C. Chi, *Angew. Chem. Int. Ed.* **2021**, *60*, 2658–2662; *Angew. Chem.* **2021**, *133*, 2690–2694.
[9] G. Povie, Y. Segawa, T. Nishihara, Y. Miyauchi, K. Itami, *Science* **2017**, *356*, 172–175.
[10] E. R. Darzi, R. Jasti, *Chem. Soc. Rev.* **2015**, *44*, 6401–6410.
[11] P. Li, T. J. Sisto, E. R. Darzi, R. Jasti, *Org. Lett.* **2014**, *16*, 182–185.
[12] Y. Segawa, A. Fukazawa, S. Matsuura, H. Omachi, S. Yamaguchi, S. Irle, K. Itami, *Org. Biomol. Chem.* **2012**, *10*, 5979–5984.
[13] M. Hermann, D. Wassy, B. Esser, *Angew. Chem. Int. Ed.* **2021**, *60*, 15743–15766; *Angew. Chem.* **2021**, *133*, 15877–15900.
[14] J. S. Wössner, D. Wassy, A. Weber, M. Bovenkerk, M. Hermann, M. Schmidt, B. Esser, *J. Am. Chem. Soc.* **2021**, *143*, 12244–12252.
[15] E. R. Darzi, E. S. Hirst, C. D. Weber, L. N. Zakharov, M. C. Lonergan, R. Jasti, *ACS Cent. Sci.* **2015**, *1*, 335–342.
[16] T. Kuwabara, J. Orii, Y. Segawa, K. Itami, *Angew. Chem. Int. Ed.* **2015**, *54*, 9646–9649; *Angew. Chem.* **2015**, *127*, 9782–9785.
[17] Y. Xu, S. Gsänger, M. B. Minameyer, I. Imaz, D. Maspoch, O. Shyshov, F. Schwer, X. Ribas, T. Drewello, B. Meyer, M. Von Delius, *J. Am. Chem. Soc.* **2019**, *141*, 18500–18507.
[18] M. Ball, B. Fowler, P. Li, L. A. Joyce, F. Li, T. Liu, D. Paley, Y. Zhong, H. Li, S. Xiao, F. Ng, M. L. Steigerwald, C. Nuckolls, *J. Am. Chem. Soc.* **2015**, *137*, 9982–9987.
[19] Y. Xu, M. von Delius, *Angew. Chem. Int. Ed.* **2020**, *59*, 559–573; *Angew. Chem.* **2020**, *132*, 567–582.
[20] N. Ozaki, H. Sakamoto, T. Nishihara, T. Fujimori, Y. Hijikata, R. Kimura, S. Irle, K. Itami, *Angew. Chem. Int. Ed.* **2017**, *56*, 11196–11202; *Angew. Chem.* **2017**, *129*, 11348–11354.
[21] T. Matsuno, M. Fujita, K. Fukunaga, S. Sato, H. Isobe, *Nat. Commun.* **2018**, *9*, 3779.
[22] P. Della Sala, C. Talotta, T. Caruso, M. De Rosa, A. Soriente, P. Neri, C. Gaeta, *J. Org. Chem.* **2017**, *82*, 9885–9889.
[23] Y. Xu, R. Kaur, B. Wang, M. B. Minameyer, S. Gsänger, B. Meyer, T. Drewello, D. M. Guldi, M. Von Delius, *J. Am. Chem. Soc.* **2018**, *140*, 13413–13420.
[24] S. Adachi, M. Shibasaki, N. Kumagai, *Nat. Commun.* **2019**, *10*, 3820.
[25] B. M. White, Y. Zhao, T. E. Kawashima, B. P. Branchaud, M. D. Pluth, R. Jasti, *ACS Cent. Sci.* **2018**, *4*, 1173–1178.
[26] T. A. Schaub, E. A. Prantl, J. Kohn, M. Bursch, C. R. Marshall, E. J. Leonhardt, T. C. Lovell, L. N. Zakharov, C. K. Brozek, S. R. Waldvogel, S. Grimme, R. Jasti, *J. Am. Chem. Soc.* **2020**, *142*, 8763–8775.
[27] R. Frydrych, T. Lis, W. Bury, J. Cybińska, M. Stépień, *J. Am. Chem. Soc.* **2020**, *142*, 15604–15613.
[28] K. Tahara, Y. Tobe, *Chem. Rev.* **2006**, *106*, 5274–5290.

[29] J. Zhu, Y. Han, Y. Ni, G. Li, J. Wu, *J. Am. Chem. Soc.* **2021**, *143*, 2716–2721.
[30] Y. Li, Y. Segawa, A. Yagi, K. Itami, *J. Am. Chem. Soc.* **2020**, *142*, 12850–12856.
[31] K. Y. Cheung, S. Gui, C. Deng, H. Liang, Z. Xia, Z. Liu, L. Chi, Q. Miao, *Chem* **2019**, *5*, 838–847.
[32] K. Senthilkumar, M. Kondratowicz, T. Lis, P. J. Chmielewski, J. Cybińska, J. L. Zafra, J. Casado, T. Vives, J. Crassous, L. Favereau, M. Stępień, *J. Am. Chem. Soc.* **2019**, *141*, 7421–7427.
[33] L. Palomo, L. Favereau, K. Senthilkumar, M. Stępień, J. Casado, F. J. Ramírez, *Angew. Chem. Int. Ed.* **2022**, *61*, e202206976; *Angew. Chem.* **2022**, *134*, e202206976.
[34] E. Kayahara, T. Iwamoto, H. Takaya, T. Suzuki, M. Fujitsuka, T. Majima, N. Yasuda, N. Matsuyama, S. Seki, S. Yamago, *Nat. Commun.* **2013**, *4*, 2694.
[35] N. Hayase, J. Nogami, Y. Shibata, K. Tanaka, *Angew. Chem. Int. Ed.* **2019**, *58*, 9439–9442; *Angew. Chem.* **2019**, *131*, 9539–9542.
[36] S. Cui, G. Zhuang, D. Lu, Q. Huang, H. Jia, Y. Wang, S. Yang, P. Du, *Angew. Chem. Int. Ed.* **2018**, *57*, 9330–9335; *Angew. Chem.* **2018**, *130*, 9474–9479.
[37] Z. Sun, K. Ikemoto, T. M. Fukunaga, T. Koretsune, R. Arita, S. Sato, H. Isobe, *Science* **2019**, *363*, 151–155.
[38] K. Ikemoto, S. Yang, H. Naito, M. Kotani, S. Sato, H. Isobe, *Nat. Commun.* **2020**, *11*, 1807.
[39] K. Ikemoto, S. Harada, S. Yang, T. Matsuno, H. Isobe, *Angew. Chem. Int. Ed.* **2022**, *61*, e202114305; *Angew. Chem.* **2022**, *134*, e202114305.
[40] H. W. Jiang, T. Tanaka, H. Mori, K. H. Park, D. Kim, A. Osuka, *J. Am. Chem. Soc.* **2015**, *137*, 2219–2222.
[41] H. Jia, G. Zhuang, Q. Huang, J. Wang, Y. Wu, S. Cui, S. Yang, P. Du, *Chem. Eur. J.* **2020**, *26*, 2159–2163.
[42] Z. Sun, T. Mio, K. Ikemoto, S. Sato, H. Isobe, *J. Org. Chem.* **2019**, *84*, 3500–3507.
[43] C. Eaborn, K. J. Odell, A. Pidock, *Dalton Trans.* **1978**, *4*, 357–368.
[44] H. Jia, Y. Gao, Q. Huang, S. Cui, P. Du, *Chem. Commun.* **2018**, *54*, 988–991.
[45] L. Sicard, F. Lucas, O. Jeannin, P. Bouit, J. Rault-Berthelot, C. Quinton, C. Poriel, *Angew. Chem. Int. Ed.* **2020**, *59*, 11066–11072; *Angew. Chem.* **2020**, *132*, 11159–11165.
[46] N. Grabicki, K. T. D. Nguyen, S. Weidner, O. Dumele, *Angew. Chem. Int. Ed.* **2021**, *60*, 14909–14914; *Angew. Chem.* **2021**, *133*, 15035–15041.
[47] Y. Tsuchido, R. Abe, T. Ide, K. Osakada, *Angew. Chem. Int. Ed.* **2020**, *59*, 22928–22932; *Angew. Chem.* **2020**, *132*, 23128–23132.
[48] Y. Yoshigoe, Y. Tanji, Y. Hata, K. Osakada, S. Saito, E. Kayahara, S. Yamago, Y. Tsuchido, H. Kawai, *JACS Au* **2022**, *2*, 1857–1868.
[49] N. Grabicki, O. Dumele, *Synlett* **2022**, *33*, 1–7.
[50] W. J. Wolf, M. S. Winston, F. D. Toste, *Nat. Chem.* **2014**, *6*, 159–164.
[51] H. A. Staab, F. Binnig, *Tetrahedron Lett.* **1964**, *5*, 319–321.
[52] D. J. Cram, T. Kaneda, R. C. Helgeson, G. M. Lein, *J. Am. Chem. Soc.* **1979**, *101*, 6752–6754.
[53] W. Pisula, M. Kastler, C. Yang, V. Enkelmann, K. Müllen, *Chem. Asian J.* **2007**, *2*, 51–56.
[54] J. M. W. Chan, T. M. Swager, *Tetrahedron Lett.* **2008**, *49*, 4912–4914.
[55] J. Y. Xue, K. Ikemoto, N. Takahashi, T. Izumi, H. Taka, H. Kita, S. Sato, H. Isobe, *J. Org. Chem.* **2014**, *79*, 9735–9739.
[56] S. M. Kim, M. H. Kim, S. Y. Choi, J. G. Lee, J. Jang, J. B. Lee, J. H. Ryu, S. S. Hwang, J. H. Park, K. Shin, Y. G. Kim, S. M. Oh, *Energy Environ. Sci.* **2015**, *8*, 1538–1543.
[57] J. Wang, Y.-Y. Ju, K.-H. Low, Y.-Z. Tan, J. Liu, *Angew. Chem. Int. Ed.* **2021**, *60*, 11814–11818; *Angew. Chem.* **2021**, *133*, 11920–11924.
[58] F. A. L. Anet, A. J. R. Bourn, *J. Am. Chem. Soc.* **1967**, *89*, 760–768.
[59] G. Fuhrmann, T. Debaerdemaeker, P. Bäuerle, *Chem. Commun.* **2003**, 948–949.
[60] S. Hitosugi, W. Nakanishi, T. Yamasaki, H. Isobe, *Nat. Commun.* **2011**, *2*, 492.
[61] L. Sicard, F. Lucas, O. Jeannin, P. A. Bouit, J. Rault-Berthelot, C. Quinton, C. Poriel, *Angew. Chem. Int. Ed.* **2020**, *59*, 11066–11072; *Angew. Chem.* **2020**, *132*, 11159–11165.
[62] H. W. Jiang, T. Tanaka, T. Kim, Y. M. Sung, H. Mori, D. Kim, A. Osuka, *Angew. Chem. Int. Ed.* **2015**, *54*, 15197–15201; *Angew. Chem.* **2015**, *127*, 15412–15416.
[63] U. Mueller, N. Darowski, M. R. Fuchs, R. Förster, M. Hellmig, K. S. Paithankar, S. Pühringer, M. Steffien, G. Zocher, M. S. Weiss, *J. Synchrotron Radiat.* **2012**, *19*, 442–449.
[64] U. Mueller, R. Förster, M. Hellmig, F. U. Huschmann, A. Kastner, P. Malecki, S. Pühringer, M. Röwer, K. Sparta, M. Steffien, M. Ühlein, P. Wilk, M. S. Weiss, *Eur. Phys. J. Plus* **2015**, *130*, 141.
[65] M. Fujitsuka, D. W. Cho, T. Iwamoto, S. Yamago, T. Majima, *Phys. Chem. Chem. Phys.* **2012**, *14*, 14585–14588.
[66] T. Iwamoto, Y. Watanabe, Y. Sakamoto, T. Suzuki, S. Yamago, *J. Am. Chem. Soc.* **2011**, *133*, 8354–8361.
[67] C. E. Colwell, T. W. Price, T. Stauch, R. Jasti, *Chem. Sci.* **2020**, *11*, 3923–3930.
[68] L. J. Barbour, *J. Appl. Crystallogr.* **2020**, *53*, 1141–1146.
[69] K. N. Houk, K. Nakamura, C. Sheu, A. E. Keating, *Science* **1996**, *273*, 627–629.
[70] K. Hermann, Y. Ruan, A. M. Hardin, C. M. Hadad, J. D. Badjić, *Chem. Soc. Rev.* **2015**, *44*, 500–514.
[71] T. Iwamoto, Y. Watanabe, T. Sadahiro, T. Haino, S. Yamago, *Angew. Chem. Int. Ed.* **2011**, *50*, 8342–8344; *Angew. Chem.* **2011**, *123*, 8492–8494.
[72] F. Ulatowski, K. Dabrowa, T. Bałakier, J. Jurczak, *J. Org. Chem.* **2016**, *81*, 1746–1756.
[73] D. Brynn Hibbert, P. Thordarson, *Chem. Commun.* **2016**, *52*, 12792–12805.
[74] S. Hashimoto, T. Iwamoto, D. Kurachi, E. Kayahara, S. Yamago, *ChemPlusChem* **2017**, *82*, 1015–1020.
[75] S. Toyota, E. Tsurumaki, *Chem. Eur. J.* **2019**, *25*, 6878–6890.
[76] D. J. Hill, M. J. Mio, R. B. Prince, T. S. Hughes, J. S. Moore, *Chem. Rev.* **2001**, *101*, 3893–4011.
[77] T. R. Cook, P. J. Stang, *Chem. Rev.* **2015**, *115*, 7001–7045.
[78] Z. J. Kinney, C. S. Hartley, *J. Am. Chem. Soc.* **2017**, *139*, 4821–4827.
[79] Deposition numbers 2209128 (for **4**), 2208548 (for **2-Au**), and 2208573 (for **1**), 2033332 (for **4b**), 2207451 (for **4c**), and 2055826 (for **3**) contain the supplementary crystallographic data for this paper. These data are provided free of charge by the joint Cambridge Crystallographic Data Centre and Fachinformationszentrum Karlsruhe Access Structures service.

Manuscript received: December 5, 2022
Accepted manuscript online: February 8, 2023
Version of record online: March 9, 2023